

## Exploring the Binding Pathway of Novel Nonpeptidomimetic Plasmeprin V Inhibitors

Raitis Bobrovs,\* Laura Drunka, Iveta Kanepe, Aigars Jirgensons, Amedeo Caffisch, Matteo Salvalaglio, and Kristaps Jaudzems

Cite This: <https://doi.org/10.1021/acs.jcim.3c00826>

Read Online

**ABSTRACT:** Predicting the interaction modes and binding affinities of virtual compound libraries is of great interest in drug development. It reduces the cost and time of lead compound identification and selection. Here we apply path-based metadynamics simulations to characterize the binding of potential inhibitors to the *Plasmodium falciparum* aspartic protease plasmeprin V (plm V), a validated antimalarial drug target that has a highly mobile binding site. The potential plm V binders were identified in a high-throughput virtual screening (HTVS) campaign and were experimentally verified in a fluorescence resonance energy transfer (FRET) assay. Our simulations allowed us to estimate compound binding energies and revealed relevant states along binding/unbinding pathways in atomistic resolution. We believe that the method described allows the prioritization of compounds for synthesis and enables rational structure-based drug design for targets that undergo considerable conformational changes upon inhibitor binding.



### INTRODUCTION

Drug discovery relies on computer-aided drug discovery (CADD) methods to accelerate this time-consuming and costly process. In addition, CADD and particularly rational (structure-based) design has gained a notable role in identifying novel potentially active chemical scaffolds (through virtual screening, docking, and similarity search), as well as in hit-to-lead optimization and fragment evolution.<sup>1–3</sup> Predicting the interaction modes and affinity of virtual compound libraries allows the prioritization of compounds for synthesis or testing and rationalizing structure–activity relationships.

A major challenge in applying structure-based drug design remains the accurate estimation of the target protein–ligand binding free energies (BFEs). This is essential for lead optimization since it is the most time- and resource-consuming step. Recent improvements in protein and ligand force fields, molecular dynamics (MD) codes, and enhanced sampling algorithms have made the calculation of relative and absolute binding free energies more accurate and accessible.<sup>4–7</sup> Currently, free energy perturbation (FEP) methods are preferred for relative binding free energy (RBFE) calculation, typically used in the hit-to-lead optimization stage.<sup>8,9</sup> Lately, significant progress has also been made in the calculation of absolute binding free energies (ABFEs) using alchemical approaches.<sup>10</sup> These advances have made ABFE calculations more accessible and attractive at the hit identification stage, as well. There are, however, several drawbacks that hamper the

widespread use of perturbation-based methods. Most notably, calculating accurate binding energies for systems that undergo considerable conformational changes or systems that contain charged and/or noncongeneric ligands is impossible due to the inability to accurately sample pharmacologically relevant conformations and describe pocket solvation/desolvation.<sup>11,12</sup>

Alternatives to perturbation-based methods are collective variable-based free energy calculation methods, like metadynamics, which permit ABFE calculation along a physical binding trajectory.<sup>7,13–24</sup> Metadynamics allows us to sample target conformations relevant to the binding process and explore transition states along the binding pathway. Besides, it is usually advantageous to understand the inhibitor binding at an atomic scale (key protein–inhibitor and protein–protein interactions, ligand flexibility, solvation effects, etc.), as information on inhibitor binding/unbinding pathway, potential transition states can provide the basis for targeted lead compound development to design compounds with higher activity and specificity.<sup>18,25,26</sup> The ability of metadynamics to sample the complete binding pathway, including target

Received: May 31, 2023

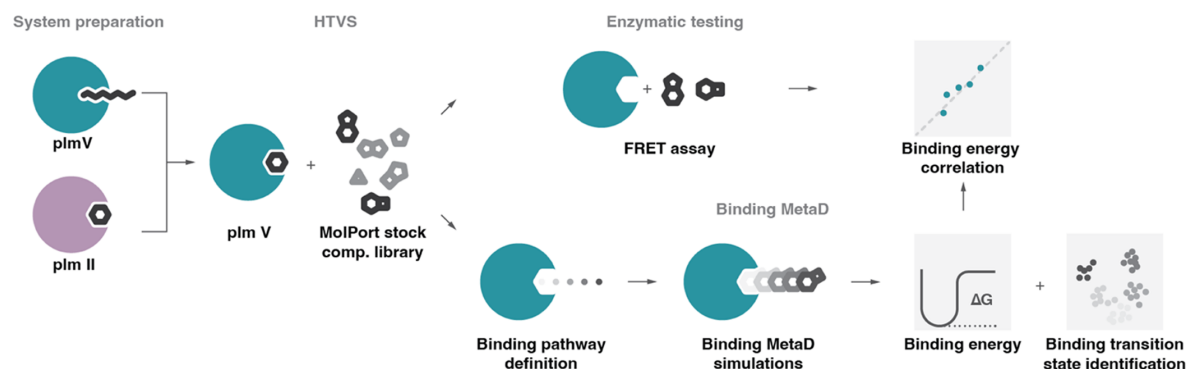


Figure 1. Schematic research workflow.

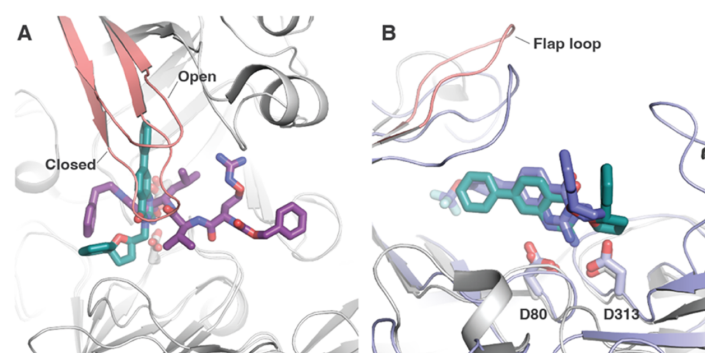


Figure 2. (A) Plm V-peptidomimetic inhibitor complex (PDB ID: 4ZL4) superimposed on plm II-nonpeptidomimetic open flap inhibitor complex (PDB ID: 4Z22). The flap loop is shown in salmon. Peptidomimetic inhibitor WEHI-842 is shown as purple sticks, nonpeptidomimetic inhibitor DR718A as teal sticks, and catalytic aspartate side chains as gray sticks. Hydrogens are omitted for clarity. (B) Plm V in complex with inhibitor DR720 after 100 ns restrained MD simulation superimposed on the plm II-DR718A complex (PDB ID: 4Z22). Plm V is shown as a violet cartoon, and plm II as a white cartoon. Catalytic aspartate side chains are shown as sticks. The plm II flap loop is shown in salmon. DR720 is shown as violet sticks, and DR718A as teal sticks. Hydrogens are omitted for clarity.

flexibility upon ligand binding and unbinding, makes it an excellent choice for ligand binding studies. In contrast, alchemical methods rely on sampling only the end states of the binding process and, thus, do not provide a mechanistic insight into how the inhibitor binds/unbinds.

Drug targets containing flexible loops next to the binding site or having cryptic or allosteric binding pockets are not uncommon.<sup>27,28</sup> One such drug target class is aspartic proteases, in which a long  $\beta$ -hairpin structure covers the binding site, usually referred to as a flap or flap loop. It is a highly mobile region that is involved in substrate recognition.<sup>29</sup> Here we applied metadynamics to study the binding of potential inhibitors to the *P. falciparum* aspartic protease plasmepsin V (plm V), a validated antimalarial drug target. The inhibitors were identified via high-throughput virtual screening, and their plm V inhibitory potency was verified experimentally. The study shows the potential of metadynamics simulations to reveal the binding modes and energies of aspartic protease inhibitors and to facilitate the discovery of new inhibitor scaffolds.

## EXPERIMENT DESIGN

Figure 1 outlines the research workflow, and critical aspects are described below. In essence, the plm V structure that enables nonpeptidomimetic inhibitor docking was prepared and used

to identify novel inhibitor scaffolds via high-throughput virtual screening (HTVS). The inhibitors identified were verified experimentally, and metadynamics simulations were applied to characterize inhibitor binding modes and energies at an atomic scale.

**System Preparation.** Plasmepsin V (plm V) is a promising, yet unexploited, antimalarial drug target. It is an essential protease that processes proteins for export into the host erythrocytes and is located in the endoplasmic reticulum.<sup>30</sup> Plm V is a phylogenetically unique aspartic protease that shares little conservation with human proteases,<sup>31–33</sup> making it less likely that its inhibitors will have selectivity issues. Most known plm V inhibitors are peptidomimetic<sup>30,33–37</sup>; for two of them, the crystal structures have been solved (PDB IDs: 4ZL4 and 6C4G; from *Plasmodium vivax*). Both structures<sup>34,35</sup> originate from complexes, where the flap loop (Tyr135-Gly147) is closed over the active site. While no plm V crystal structure in complex with a nonpeptidomimetic inhibitor has been reported, it is known that binding of such inhibitors to other aspartic proteases can lead to conformations with the flap loop in a more open state (PDB codes 4Z22 and 2BJU).<sup>38</sup> Since we were interested in identifying nonpeptidomimetic plm V inhibitors that could bind to the open flap conformation, we prepared a docking model that would be able to accommodate

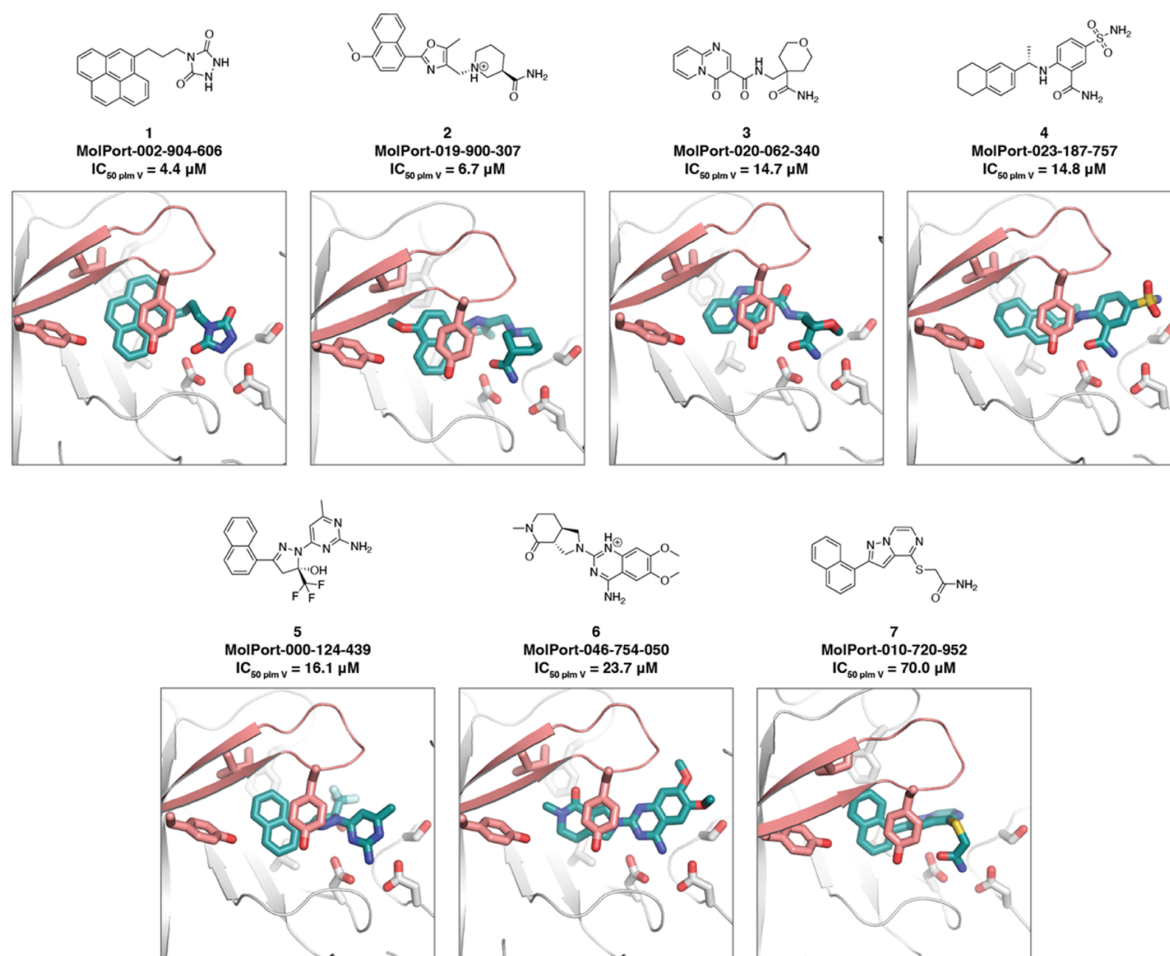


**Figure 3.** Virtual screening hits against plm V. Compound molecular structure in its highest scoring protonation state, MolPort ID, and experimental IC<sub>50</sub> value (μM) against plm V are given on top; the docked pose of the respective compound in complex with plm V is given at the bottom. Inhibitor and key amino acid residues are shown as teal and gray sticks, respectively. The flap loop is shown in salmon. Hydrogens are omitted for clarity.

such inhibitors. To do this, a moderately active plm V inhibitor (2-amino-4(3H)-quinazolinone DR720, IC<sub>50</sub> = 64 μM), identified from our in-house aspartic protease inhibitor library,<sup>39–43</sup> was modeled in the active site of plm V in a pose similar to that of another 2-amino-4(3H)-quinazolinone in complex with plm II (PDB ID 4Z22) (see Figure 2). The Asp80 of the catalytic dyad was protonated, whereas Asp313 was deprotonated.<sup>44</sup> This system was subjected to molecular dynamics simulation with an aspartic dyad and 2-amino-4(3H)-quinazolinone core intermolecular distances restrained (see the SI Section 1).

**HTVS.** The minimized protein structure was used in a high-throughput virtual screening (HTVS) of the drug-like screening compounds from the MolPort stock compound library (~6 M comp.; 2020). Molecular docking was performed using Glide, with scaling of the van der Waals radii set to 0.9 for protein and ligand heavy atoms, and docking compounds flexibly (see the SI Section 1 in the Supporting information for more information). To retain only the unique virtual screening hit scaffolds (i.e., the top-scoring compound

from each cluster), the top 3000 compounds scored were clustered by applying Tanimoto similarity metrics to linear molecule fingerprints. The top 300 compounds were visually inspected for their ability to form hydrogen bonds with the catalytic dyad and hydrophobic interactions with the flap pocket residues. Molecules showing internal strains or unsatisfied hydrogen bond donors were deprioritized. A total of 28 potential plm V binders were selected for purchase.

**Binding Metadynamics.** The inhibitor binding/unbinding pathway and respective binding energy were calculated by using fully atomistic molecular dynamics simulations. This approach describes the movement of flexible protein parts near the binding site and considers the buried pocket solvation–desolvation during the inhibitor binding/unbinding event. Since inhibitor binding is a rare event and typically is far beyond the reach of typical atomistic simulations, we exploited an enhanced sampling method called metadynamics (metaD). MetaD is a method where molecular dynamics simulation is biased along a set of collective variables (CVs) using a history-dependent potential. The Gaussian-shaped potential is applied

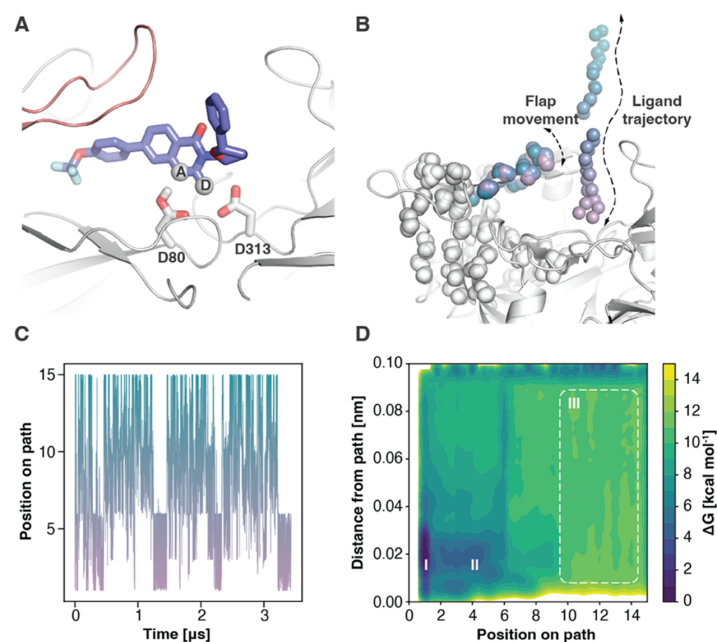


**Figure 4.** (A) Ligand transition state mimetic group hydrogen bond donor (D) and acceptor (A) atoms used to define ligand position on the binding/unbinding path depicted on the plm V-DR720 complex. The flap loop is shown in salmon. DR720 is shown as violet sticks and catalytic aspartate side chains as gray sticks. Hydrogens are omitted for clarity. (B) Fifteen superimposed frames define the ligand binding/unbinding pathway. Atoms defining path (shown as spheres) are  $C\alpha$  atoms of residues involved in  $\beta$ -sheet secondary structures within 1.5 nm from Ser87, and ligand atoms (A, D) from subfigure (A). Color gradient shows progress along the binding/unbinding pathway, where purple conformation corresponds to the bound state, teal—unbound. (C) System position on the binding/unbinding path as a function of metadynamics simulation time in the case of the plm V-comp.4 system. Colors correspond to the states given in subfigure B: purple—bound state; teal—unbound. (D) FES of compound 4 binding to plm V was obtained after reweighing<sup>48</sup> PathMetaD simulation. Isosurfaces are shown every 1 kcal/mol. The deepest FES basin I corresponds to the bound state, similar to the docked pose. Basin II corresponds to the protein–ligand encounter state where the ligand interacts with the plm V flap loop, whereas state III corresponds to the unbound state where the ligand is not interacting with the protein.

at regular intervals to escape any local minima along the CV space and to visit previously unexplored regions in the CV space. Selecting the appropriate CVs for the process studied is crucial and often is the most challenging step. The most apparent CV in the ligand–protein binding studies is the distance between the ligand and binding site atoms. This CV alone, however, is unsuitable for systems where the protein binding site is highly flexible, as it has no control over the protein binding site flexibility and might result in situations where the protein conformational space of interest is poorly explored. The intermolecular distance CV can be combined with CVs that describe protein flexibility.<sup>22,45</sup> However, since the computational cost to reconstruct the free energy surface (FES) grows exponentially with the number of CVs used, it is undesirable.

To overcome the limitations above, we used path CV that enables the exploration of complex multidimensional processes along a predefined pathway. In this method, two CVs describe the process:  $s$ , the progress along the predefined reference path, and  $z$ , the distance orthogonal to the reference path. Furthermore, introducing CV  $z$  allows the exploration of configurations that differ from the reference path; thus, if the reference path provided is not entirely accurate, the system can deviate from it and discover more probable pathways.

## RESULTS

**Virtual Screening.** Following the virtual screening approach described above, we selected and purchased 28 chemically diverse top-scoring compounds. These compounds were tested for plm V inhibition potency in a FRET-based assay, and 7 showed micromolar potency ( $IC_{50}$  in the range from 4.4 to 70  $\mu$ M; see Figure 3; complete list of tested inhibitors in Table S11). Additionally, the inhibition potency of three cross-inhibition markers, human cathepsin D (catD) and digestive plasmepsins II and IV, was measured for the compounds that showed measurable activity against plm V. Compounds 1, 5, and 6 showed considerable selectivity and no inhibition of cross-inhibition markers was observed at 100  $\mu$ M concentration (see Table S11). Identification of compounds that show selectivity over human cathepsin D prompted preliminary structure–activity relationship (SAR) studies of commercially available 1, 5, and 6 analogues which were outside the scope of the project and are summarized in SI Section 2.1.

All of the hits identified had several common features: (a) hydrogen bond donor and acceptor in a configuration that mimics the transition state of an enzymatic reaction and is capable of forming hydrogen bonds with catalytic dyad; and (b) hydrophobic substituent forming hydrophobic interactions under the flap loop once the ligand core hydrogen bond donor and acceptor groups are interacting with the catalytic site. The transition state mimicking group alignment in the binding site

D



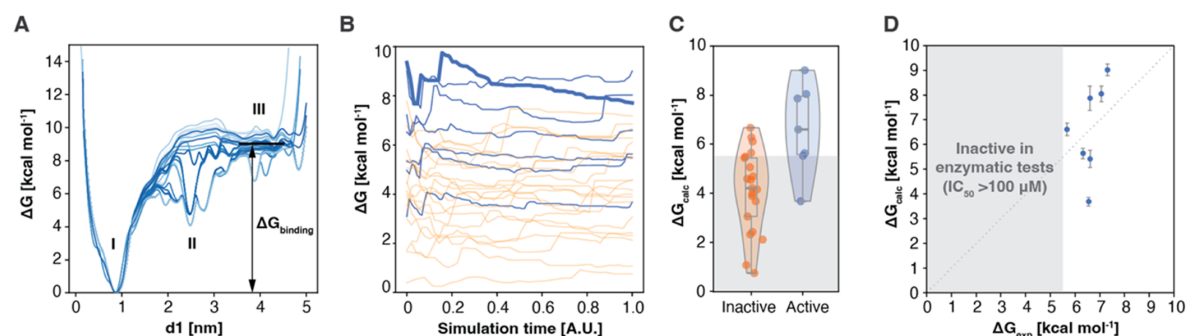


**Figure 5.** (A) FES as a function of ligand core–aspartic dyad distance  $d1$  obtained by reweighting the metadynamics simulation every 50 ns (for comp. 4). The color gradient indicates reweighting time: the lightest blue line—reweighting up to 50 ns; the darkest blue—reweighting up to 3.0  $\mu$ s. The binding site region is up to  $\sim 1$  nm, while fully solvated at  $>3$  nm. FES basing numbering is consistent with Figure 4D. (B) The binding free energy ( $\Delta G$ ) of the HTVS hits, and plm V is calculated every 50 ns throughout the simulation. Blue indicates verified inhibitors and orange indicates inactive compounds. The thick blue line represents the reference comp. 4. The compound 4 estimated binding energy of  $-7.8 \pm 0.5$  kcal/mol is slightly higher than the experimental value (calculated from the  $IC_{50}$ ) of  $\sim -6.6$  kcal/mol. (C) The violin plots of estimated binding free energy ( $\Delta G_{\text{calc}}$ ) for the experimentally verified active and inactive compounds. Gray-shaded area indicates binding free energy corresponding to  $IC_{50} > 100 \mu\text{M}$ . (D) The estimated binding free energy ( $\Delta G_{\text{calc}}$ ) plotted against experimentally determined ( $\Delta G_{\text{exp}}$ ) values (calculated from  $IC_{50}$  values as  $\Delta G_{\text{exp}} = -k_B T \ln(IC_{50})$ ).

matches other nonpeptidomimetic aspartic protease inhibitors, where ligand hydrogen bond donor and acceptor bind coplanarly with aspartic dyad residues. The most commonly observed functional group interacting with the aspartic dyad was primary amide, whereas heterocyclic compound cores were represented by quinazoline-2-amine, pyrimidine-2-amine, and triazolidione. Quinazolin-2-amines and pyrimidine-2-amines with substituents at various positions have been reported as aspartic protease inhibitors before,<sup>43,46</sup> whereas triazolidione and primary amide-based compounds, to our knowledge, are novel. The hydrophobic substituents were predominantly aromatic systems interacting with flap pocket residues Tyr135, Tyr139, Ile145, Phe180, and Val188. In addition to the interactions mentioned above, compounds 4 and 6 interacted with the Ser316 side chain, forming hydrogen bonds via sulfonamide and methoxy groups, respectively.

**Binding Energy and Pathway Calculation.** Once a set of verified plm V inhibitors and inactive compounds was identified, studies focused on characterizing the compound binding at a molecular scale. Ligand binding pathway studies were initiated by creating a reference ligand binding/unbinding path, which was generated from a trajectory obtained during an initial funnel metadynamics simulation (comp. DR720 unbinding from plm V; see SI Section 1). It consisted of 15 equally spaced configurations, prepared using Plumed<sup>47</sup> pathools. The  $C\alpha$  atoms of the binding site (within 15 Å from Ser87, which sits under the central part of the flap loop) and two ligand atoms were used to define a path describing both the binding site flexibility and ligand position during the binding process. The two ligand atoms defined within the path were hydrogen bond donor and acceptor groups interacting with catalytic aspartates. This configuration allowed us to use the same path for all potential inhibitor simulations and specify the ligand orientation with respect to the binding site. During the preliminary runs, it was observed that ligands occasionally deviated considerably from the path provided. Therefore, upper wall restraint potential was introduced at RMSD 0.1 nm for the CV  $z$ . This allowed the ligand to explore the binding pocket while restricting the space explored in the unbound state.

The PathMetaD simulations were performed for all 28 ligands considered, ranging in simulation time from 1 to 3  $\mu$ s. During these simulations, multiple ligand binding and unbinding events were observed, and ligands explored both bound and unbound states (frames 1–3 and 13–15 on the path, respectively; see Figure 4B,C). The unbiased probability distribution of the system was obtained through reweighting,<sup>48</sup> which allowed us to construct the FES associated with the binding process (see Figure 4D; the FES for the rest of the verified plm V inhibitors is given in Figure S11) and calculate the ligand binding free energy. A randomly selected, verified plm V inhibitor (compound 4) was used to optimize metaD parameters (see the SI Section 1) and is used as a representative case throughout the study.

The converged ligand binding/unbinding trajectories were used to calculate ligand binding free energies and identify key protein–ligand encounter states along the binding pathway.

**Ligand Binding Free Energy.** The ligand binding free energy was calculated as a difference between the global minima that represent the state where the ligand is interacting with the catalytic dyad (state I) and the mean energy of the state where the ligand is completely solvent exposed and does not interact with the protein (state III) (see Figures 4D and 5A). The ligand binding mode corresponding to the global FES minima I identified in PathMetaD simulations generally was in line with the docked pose for the verified plm V inhibitors, with ligand heavy atom RMSD values ranging from 2 to 5 with respect to docked poses (see binding pose comparison in Figure S12). Notably, the unbound region III is flat, indicating the presence of isoenergetic states once the ligand is sufficiently distant from the protein. The convergence of the binding energy was estimated by monitoring the evolution of the absolute binding free energy throughout the simulation (Figure 5A,B). Figure 5 shows that for the plm V-compound 4 system, the free energy converges after  $\sim 1000$  ns. Similar behavior was observed for the rest of the inhibitors.

The  $IC_{50}$  values were determined for the compounds with more than 50% plm V inhibition at 100  $\mu\text{M}$  concentration. For these verified active compounds, it was possible to estimate the experimental ligand binding energy as  $\Delta G_{\text{exp}} = -k_B T \ln(IC_{50})$ .

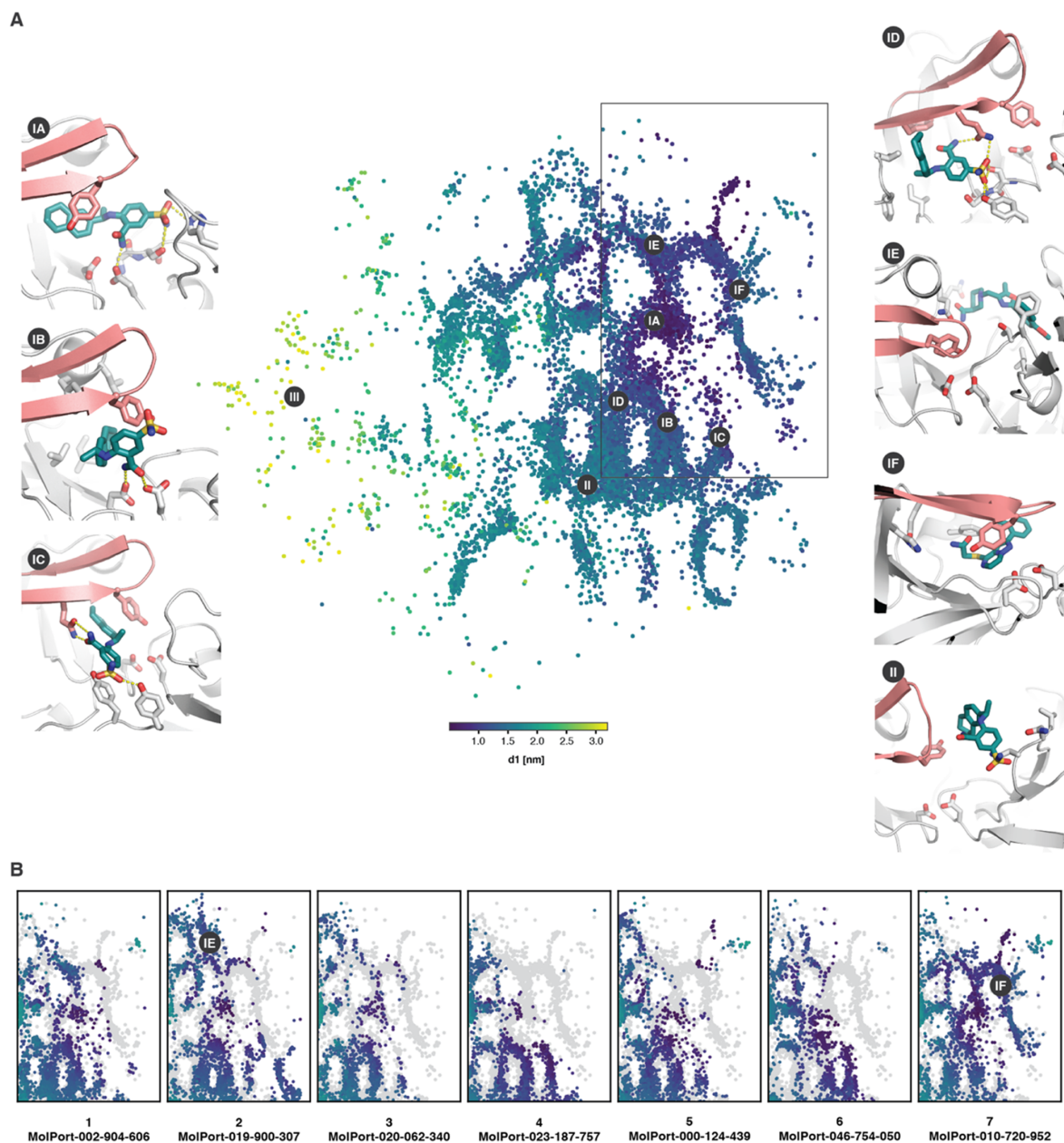


**Figure 6.** (A) Sketch map of combined verified plm V inhibitor binding to plm V was obtained by mapping the binding trajectory's three-dimensional space to a 2D representation. The map is color-coded according to ligand core–catalytic dyad distance  $d_1$ . The key states along the binding pathway are indicated as IA–F and II, and the unbound state as III. The rectangle indicates the region where the inhibitor interacts with the binding site residues and is compared in subfigure (B). The corresponding binding modes along the binding pathway are shown alongside the map. The ligand is shown as green sticks, selected binding pocket residues and catalytic dyad residues are shown as gray sticks, and the flap loop is in salmon. Hydrogens are omitted for clarity. (B) Comparison of experimentally verified plm V inhibitor binding sketch maps and reference map shown in subfigure (A). Gray, reference sketch map from subfigure (A). The color coding matches subfigure (A).

The violin plots (Figure 5C) of the estimated binding free energy ( $\Delta G_{\text{calc}}$ ) indicate that the PathMetaD binding energy estimate allows us to distinguish experimentally verified active and inactive compounds. Moreover, the scatter plot of the calculated and experimental binding energy (Figure 5D) demonstrates that PathMetaD binding energy estimate falls

within  $\sim 1.3$  kcal/mol of experimental data (all calculated and estimated binding energies are summarized in Table S12). Such accuracy is comparable to other MD-based binding energy calculation methods.<sup>49</sup> The one distinct outlier for the enzymatically verified plm V inhibitors is the binding energy estimate for the comp. 5 with a calculated binding free energy

of  $-3.7$  kcal/mol versus the experimental value of  $-6.5$  kcal/mol. The calculated binding energies for the experimentally verified inactive compounds ranged from  $-0.76$  to  $-6.68$  kcal/mol. According to the above equation, these compounds' free energy of binding should be less negative than  $-5.5$  kcal/mol (since  $IC_{50} > 100 \mu M$ ). Four experimentally verified inactive compounds showed slightly better binding energy. The accuracy of the binding energy estimate is typically hindered by insufficient sampling and imperfect force field parameters. Here, the ligand extensively explored both bound and unbound states (Figure 4C). Therefore, contributions from even minor parameter imprecisions in the protein force field, protonation state, ligand parametrization, and water model could cause unexpected outcomes.

**Binding Modes.** Besides the lowest energy state I in Figure 4D, an additional basin (basin II in Figure 4D) was observed for most ligands, indicating the presence of transition state(s) along the ligand binding pathway. While path CVs easily discriminate between the bound and unbound states, they do not provide in-depth information on the binding mode(s) and possible transition states. Such information, however, can often be accessed by reweighing the trajectory and reconstructing the FES as a function of alternative CVs that allow for decoupling states that otherwise would overlap in the initial CV space. Here, reweighing the trajectory to construct FES as a function of ligand–protein catalytic site distance  $d1$  and ligand torsion with respect to protein binding site  $t1$  (see Figure SI4) did not provide clear information on key transition states along the binding pathway. The FES constructed had broad global minima corresponding to two similar binding modes, one in a pose similar to the docked one (basin IA in Figure SI4C) and another with hydrophobic flap pocket substituent slightly twisted to fill S3 pocket (basin IB in Figure SI4C). No information was obtained on intermediate state II observed in the biased path CV space ( $s, z$ ) and one-dimensional FES (distance  $d1$ ) at  $\sim 2.5$  nm. Therefore, a dimensionality reduction method that allows for the mapping of high-dimensional processes to low-dimensional space was employed. Here we exploited the nonlinear dimensionality reduction algorithm sketch map, based on metric multidimensional scaling and specifically designed to deal with atomistic simulation data.<sup>50,51</sup> This method accurately reproduces the relative positions of adjacent basins and can often generate an intuitive representation of complex pathways. The two-dimensional (2D) map generated (using data from all verified plm V inhibitor simulations; see the SI Section 1) and representative structures are shown in Figure 6. Here, numerous well-localized basins were identified, and basins that contain structures that are expected to be next to each other on a binding pathway are located in close proximity and connections between these clusters become visible. For example, the binding mode with a ligand slightly twisted and hydrophobic substituent filling the S3 pocket (basin IB; see Figure SI3 for the aspartic protease binding site subpocket naming scheme), as well as clusters representing transition states where the ligand is next to the catalytic dyad but interacting with a flap loop (basins IC and ID in Figure 6A) are located next to the bound state basin IA. Basins located further from the bound state correspond to states in which the ligand is outside the binding site. The most populated of these is basin II, where the inhibitor interacts with a flap loop tip and flexible loop on the opposite side of the binding groove.<sup>38</sup> This is the first ligand and protein encounter on the binding

pathway. Interactions formed here guide the ligand deeper into the binding site to finally form hydrogen bonds with the catalytic dyad. Configurations corresponding to the unbound ligand state (basin III) are widespread, indicating no preferred configuration once the ligand is away from the protein.

Similar binding pathways are expected for all of the inhibitors identified. Therefore, trajectories of verified plm V inhibitors were projected on top of the reference sketch map discussed before (see Figure 6B). All inhibitors have several binding modes captured in the reference sketch map. Basins IA, IB, IC, and ID were observed for all the ligands studied; however, the population of each of them varies from ligand to ligand. The most populated basin for all ligands except comp. 6 was ID, where the inhibitor is situated right next to the flap loop in a hydrophobic groove. For comp. 6, the most populated were basins IB and IC, where ligand flap loop substituent is located under the flap and fills the S3 pocket. Basin IC was one of the most populated basins for comp. 4 and 6, while it was mostly under-represented for the rest of the ligands. This, most likely, was because only 4 and 6 can simultaneously interact with flap loop Gln173 and nearby Tyr286. The basin IA represents configurations similar to the docked ones, with a minor difference in that the flap loop substituent is slightly twisted to partly interact in the hydrophobic region right next to the flap.

Besides binding modes observed for all studied ligands, additional binding modes IE and IF were observed for comp. 2 and 7, respectively. Basin IE corresponds to the transition state where the inhibitor core interacts with Gln183 and/or Gln184 in a substrate binding groove, whereas basin IF corresponds to the binding mode where the inhibitor transition state mimetic group is wedged between the flap loop and nearby  $\alpha$  helix. Here inhibitor hydrogen bond donor and acceptor groups form hydrogen bonds with His173 and Glu176, and the flap pocket substituent is involved in aromatic stacking with Phe180 (see Figure SI2).<sup>51,52</sup>

## CONCLUSIONS

We have presented here a method for inhibitor binding free energy estimation and protein–ligand encounter state identification. The method was applied to characterize compound binding to validated antimalarial drug target *Plasmodium falciparum* aspartic protease plasmepsin V. The proposed approach utilizes path metadynamics, where the process of interest is studied by exploring the space of unbinding paths starting from a predefined reference one. Here, the reference path that describes inhibitor binding contains not only the coordinates of the potential inhibitor but also the coordinates of selected binding site residue atoms to sample relevant target conformations. This is one of the most significant advantages of the proposed method, as it accurately characterizes binding to flexible targets, which is typically problematic using free energy perturbation-based methods.

Furthermore, metadynamics CV selection and parameter optimization usually are tedious and time-consuming. Therefore, the fact that the proposed approach allows the same binding path for all compounds of interest greatly simplifies the simulation setup. The method also enables sampling complete inhibitor binding and unbinding pathways, including relevant transition states that might provide additional information for targeted lead compound development.

Moreover, we also demonstrated an approach to identify states that are shared between various structurally unrelated



inhibitors (or are unique to a specific inhibitor) using the dimensionality reduction method sketch map. This could be particularly useful in lead compound selection to identify inhibitors that meet a specific requirement. In addition to demonstrating the method's applicability, the study provides new, verified plasmepsin V inhibitor scaffolds that can be further developed into potential antimalarials. Overall, our results suggest that it is possible to use a path-metadynamics-based approach to study systems where inhibitor binding is associated with considerable conformational changes. This technique can be easily deployed to determine accurate binding free energies. We believe that the approach described might prove useful in drug development pipelines where the binding of a large set of structurally diverse ligands needs to be characterized.

## ■ ASSOCIATED CONTENT

### Supporting Information

The Supporting Information is available free of charge at <https://pubs.acs.org/doi/10.1021/acs.jcim.3c00826>.

Figures illustrating parameters used for MetaD simulation reweighing; relevant inhibitor–protein binding modes; enzymatic activity data; computational and experimental methods used (PDF)

## ■ AUTHOR INFORMATION

### Corresponding Author

Raitis Bobrovs – Latvian Institute of Organic Synthesis, Riga LV1006, Latvia; [orcid.org/0000-0002-0221-8658](https://orcid.org/0000-0002-0221-8658);  
Email: [raitis.bobrovs@osi.lv](mailto:raitis.bobrovs@osi.lv)

### Authors

Laura Drunka – Latvian Institute of Organic Synthesis, Riga LV1006, Latvia

Iveta Kanepe – Latvian Institute of Organic Synthesis, Riga LV1006, Latvia

Aigars Jirgensons – Latvian Institute of Organic Synthesis, Riga LV1006, Latvia; [orcid.org/0000-0002-8937-8792](https://orcid.org/0000-0002-8937-8792)

Amedeo Cafilisch – Department of Biochemistry, University of Zurich, CH-8057 Zurich, Switzerland; [orcid.org/0000-0002-2317-6792](https://orcid.org/0000-0002-2317-6792)

Matteo Salvalaglio – Thomas Young Centre and Department of Chemical Engineering, University College London, London WC1E 7JE, United Kingdom; [orcid.org/0000-0003-3371-2090](https://orcid.org/0000-0003-3371-2090)

Kristaps Jaudzems – Latvian Institute of Organic Synthesis, Riga LV1006, Latvia; [orcid.org/0000-0003-3922-2447](https://orcid.org/0000-0003-3922-2447)

Complete contact information is available at:

<https://pubs.acs.org/doi/10.1021/acs.jcim.3c00826>

### Notes

The authors declare no competing financial interest. Metadynamics simulations were performed using open-source software Gromacs2021 (<https://www.gromacs.org/>) patched with Plumed2.7.2 (<https://www.plumed.org/>). Plumed input files used in this work are available via PLUMED-NEST<sup>52</sup> (<https://www.plumed-nest.org>), the public repository for the Plumed consortium, using the project plumID: 23.019. Protein structures used in this study were retrieved from the RCSB protein data bank (<https://www.rcsb.org/>). Figures were prepared using PyMOL2.5.2 (<https://pymol.org/2/>), and data were plotted using matplotlib (<https://matplotlib.org/>)

## ■ ACKNOWLEDGMENTS

R.B. acknowledges the European Regional Development Fund Project No. 1.1.1.2/VIAA/2/18/379 for financial support. Calculations were partly performed in Riga Technical University (RTU) High-Performance Computing (HPC) Centre facilities. Gareth Tribello is acknowledged for his help with the sketch map calculation setup.

## ■ REFERENCES

- (1) Suryanarayanan, V.; Panwar, U.; Chandra, I. *Computational Drug Discovery and Design*; Springer, 2018; Vol. 1762.
- (2) Kuhn, B.; Guba, W.; Hert, J.; Banner, D.; Bissantz, C.; Ceccarelli, S.; Haap, W.; Körner, M.; Kuglstatter, A.; Lerner, C.; Mattei, P.; Neidhart, W.; Pinard, E.; Rudolph, M. G.; Schulz-Gasch, T.; Woltering, T.; Stahl, M. A Real-World Perspective on Molecular Design. *J. Med. Chem.* **2016**, *59* (9), 4087–4102.
- (3) Wermuth, C. G. Ring Transformations. In *The Practice of Medicinal Chemistry*, 3rd ed.; Wermuth, C. G., Ed.; Academic Press, 2008; Chapter 16.
- (4) Abraham, M. J.; Murtola, T.; Schulz, R.; Páll, S.; Smith, J. C.; Hess, B.; Lindahl, E. Gromacs: High Performance Molecular Simulations through Multi-Level Parallelism from Laptops to Supercomputers. *SoftwareX* **2015**, *1–2*, 19–25.
- (5) Laio, A.; Parrinello, M. Escaping Free-Energy Minima. *Proc. Natl. Acad. Sci. U.S.A.* **2002**, *99* (20), 12562–12566.
- (6) Wang, J.; Wolf, R. M.; Caldwell, J. W.; Kollman, P. A.; Case, D. A. Development and Testing of a General Amber Force Field. *J. Comput. Chem.* **2004**, *25* (9), 1157–1174.
- (7) Limongelli, V.; Bonomi, M.; Parrinello, M. Funnel Metadynamics as Accurate Binding Free-Energy Method. *Proc. Natl. Acad. Sci. U.S.A.* **2013**, *110* (16), 6358–6363.
- (8) Williams-Noonan, B. J.; Yuriev, E.; Chalmers, D. K. Free Energy Methods in Drug Design: Prospects of “Alchemical Perturbation” in Medicinal Chemistry. *J. Med. Chem.* **2018**, *61* (3), 638–649.
- (9) Wang, L.; Wu, Y.; Deng, Y.; Kim, B.; Pierce, L.; Krilov, G.; Lupyán, D.; Robinson, S.; Dahlgren, M. K.; Greenwood, J.; Romero, D. L.; Masse, C.; Knight, J. L.; Steinbrecher, T.; Beuming, T.; Damm, W.; Harder, E.; Sherman, W.; Brewer, M.; Wester, R.; Murcko, M.; Frye, L.; Farid, R.; Lin, T.; Mobley, D. L.; Jorgensen, W. L.; Berne, B. J.; Friesner, R. A.; Abel, R. Accurate and Reliable Prediction of Relative Ligand Binding Potency in Prospective Drug Discovery by Way of a Modern Free-Energy Calculation Protocol and Force Field. *J. Am. Chem. Soc.* **2015**, *137* (7), 2695–2703.
- (10) Rizzi, A.; Murkli, S.; McNeill, J. N.; Yao, W.; Sullivan, M.; Gilson, M. K.; Chiu, M. W.; Isaacs, L.; Gibb, B. C.; Mobley, D. L.; Chodera, J. D. Overview of the SAMPL6 Host–Guest Binding Affinity Prediction Challenge. *J. Comput.-Aided Mol. Des.* **2018**, *32* (10), 937–963.
- (11) Michel, J.; Essex, J. W. Prediction of Protein–Ligand Binding Affinity by Free Energy Simulations: Assumptions, Pitfalls and Expectations. *J. Comput.-Aided Mol. Des.* **2010**, *24* (8), 639–658.
- (12) Lapelosa, M.; Gallicchio, E.; Levy, R. M. Conformational Transitions and Convergence of Absolute Binding Free Energy Calculations. *J. Chem. Theory Comput.* **2012**, *8* (1), 47–60.
- (13) Evans, R.; Hovan, L.; Tribello, G. A.; Cossins, B. P.; Estarellas, C.; Gervasio, F. L. Combining Machine Learning and Enhanced Sampling Techniques for Efficient and Accurate Calculation of Absolute Binding Free Energies. *J. Chem. Theory Comput.* **2020**, *16* (7), 4641–4654.
- (14) Bernetti, M.; Masetti, M.; Recanatini, M.; Amaro, R. E.; Cavalli, A. An Integrated Markov State Model and Path Metadynamics Approach to Characterize Drug Binding Processes. *J. Chem. Theory Comput.* **2019**, *15* (10), 5689–5702.
- (15) Raniolo, S.; Limongelli, V. Ligand Binding Free-Energy Calculations with Funnel Metadynamics. *Nat. Protoc.* **2020**, *15* (9), 2837–2866.
- (16) Deganutti, G.; Moro, S.; Reynolds, C. A. A Supervised Molecular Dynamics Approach to Unbiased Ligand–Protein



Unbinding. *J. Chem. Inf. Model.* **2020**, 1804–1817, DOI: 10.1021/acs.jcim.9b01094.

(17) Evenseth, L. S. M.; Ocello, R.; Gabrielsen, M.; Masetti, M.; Recanatini, M.; Sylte, I.; Cavalli, A. Exploring Conformational Dynamics of the Extracellular Venus Flytrap Domain of the GABAB Receptor: A Path-Metadynamics Study. *J. Chem. Inf. Model.* **2020**, 60 (4), 2294–2303.

(18) Bobrovs, R.; Basens, E. E.; Drunka, L.; Kanepe, I.; Matisone, S.; Velins, K. K.; Andrianov, V.; Leitis, G.; Zelencova-Gopejenko, D.; Rasina, D.; Jirgensons, A.; Jaudzems, K. Exploring Aspartic Protease Inhibitor Binding to Design Selective Antimalarials. *J. Chem. Inf. Model.* **2022**, 62 (13), 3263–3273.

(19) Mattei, G.; Deflorian, F.; Mason, J. S.; De Graaf, C.; Gervasio, F. L. Understanding Ligand Binding Selectivity in a Prototypical GPCR Family. *J. Chem. Inf. Model.* **2019**, 59 (6), 2830–2836.

(20) Cavalli, A.; Spitaleri, A.; Saladino, G.; Gervasio, F. L. Investigating Drug-Target Association and Dissociation Mechanisms Using Metadynamics-Based Algorithms. *Acc. Chem. Res.* **2015**, 48 (2), 277–285.

(21) Callea, L.; Bonati, L.; Motta, S. Metadynamics-Based Approaches for Modeling the Hypoxia-Inducible Factor  $2\alpha$  Ligand Binding Process. *J. Chem. Theory Comput.* **2021**, 17 (7), 3841–3851.

(22) Tiwary, P.; Limongelli, V.; Salvalaglio, M.; Parrinello, M. Kinetics of Protein-Ligand Unbinding: Predicting Pathways, Rates, and Rate-Limiting Steps. *Proc. Natl. Acad. Sci. U.S.A.* **2015**, 112 (5), E386–E391.

(23) Tiwary, P.; Parrinello, M. From Metadynamics to Dynamics. *Phys. Rev. Lett.* **2013**, 111 (23), No. 230602, DOI: 10.1103/PhysRevLett.111.230602.

(24) Bertazzo, M.; Gobbo, D.; Decherchi, S.; Cavalli, A. Machine Learning and Enhanced Sampling Simulations for Computing the Potential of Mean Force and Standard Binding Free Energy. *J. Chem. Theory Comput.* **2021**, 17 (8), 5287–5300.

(25) Lotz, S. D.; Dickson, A. Unbiased Molecular Dynamics of 11 min Timescale Drug Unbinding Reveals Transition State Stabilizing Interactions. *J. Am. Chem. Soc.* **2018**, 140 (2), 618–628.

(26) Tiwary, P.; Mondal, J.; Berne, B. J. How and When Does an Anticancer Drug Leave Its Binding Site? *Sci. Adv.* **2017**, 3 (5), No. e1700014, DOI: 10.1126/sciadv.1700014.

(27) Christopoulos, A. Allosteric Binding Sites on Cell-Surface Receptors: Novel Targets for Drug Discovery. *Nat. Rev. Drug Discovery* **2002**, 1 (3), 198–210.

(28) Durrant, J. D.; McCammon, J. A. Molecular Dynamics Simulations and Drug Discovery. *BMC Biol.* **2011**, 9, No. 71, DOI: 10.1186/1741-7007-9-71.

(29) Goldberg, D. E. Hemoglobin Degradation. In *Current Topics in Microbiology and Immunology*; Springer, 2005; Vol. 295, pp 275–291 DOI: 10.1007/3-540-29088-5\_11.

(30) Sleebs, B. E.; Lopaticki, S.; Marapana, D. S.; O'Neill, M. T.; Rajasekaran, P.; Gazdik, M.; Günther, S.; Whitehead, L. W.; Lowes, K. N.; Barford, L.; Hviid, L.; Shaw, P. J.; Hodder, A. N.; Smith, B. J.; Cowman, A. F.; Boddey, J. A. Inhibition of Plasmepepsin V Activity Demonstrates Its Essential Role in Protein Export, PfEMP1 Display, and Survival of Malaria Parasites. *PLoS Biol.* **2014**, 12 (7), No. e1001897.

(31) Russo, L.; Babbitt, S.; Muralidharan, V.; Butler, T.; Oksman, A.; Goldberg, D. E. Plasmepepsin v Licenses Plasmodium Proteins for Export into the Host Erythrocyte. *Nature* **2010**, 463 (7281), 632–636.

(32) Boddey, J. A.; Hodder, A. N.; Günther, S.; Gilson, P. R.; Patsiouras, H.; Kapp, E. A.; Pearce, J. A.; De Koning-Ward, T. F.; Simpson, R. J.; Crabb, B. S.; Cowman, A. F. An Aspartyl Protease Directs Malaria Effector Proteins to the Host Cell. *Nature* **2010**, 463 (7281), 627–631.

(33) Sleebs, B. E.; Gazdik, M.; O'Neill, M. T.; Rajasekaran, P.; Lopaticki, S.; Lackovic, K.; Lowes, K.; Smith, B. J.; Cowman, A. F.; Boddey, J. A. Transition State Mimetics of the Plasmodium Export Element Are Potent Inhibitors of Plasmepepsin V from *P. falciparum* and *P. vivax*. *J. Med. Chem.* **2014**, 57 (18), 7644–7662.

(34) Nguyen, W.; Hodder, A. N.; de Lezongard, R. B.; Czabotar, P. E.; Jarman, K. E.; O'Neill, M. T.; Thompson, J. K.; Jousset Sabroux, H.; Cowman, A. F.; Boddey, J. A.; Sleebs, B. E. Enhanced Antimalarial Activity of Plasmepepsin V Inhibitors by Modification of the P2 position of PEXEL Peptidomimetics. *Eur. J. Med. Chem.* **2018**, 154, 182–198.

(35) Hodder, A. N.; Sleebs, B. E.; Czabotar, P. E.; Gazdik, M.; Xu, Y.; O'Neill, M. T.; Lopaticki, S.; Nebl, T.; Triglia, T.; Smith, B. J.; Lowes, K.; Boddey, J. A.; Cowman, A. F. Structural Basis for Plasmepepsin v Inhibition That Blocks Export of Malaria Proteins to Human Erythrocytes. *Nat. Struct. Mol. Biol.* **2015**, 22 (8), 590–596.

(36) Gambini, L.; Rizzi, L.; Pedretti, A.; Tagliatala-Scafati, O.; Carucci, M.; Pancotti, A.; Galli, C.; Read, M.; Giuriso, E.; Romeo, S.; Russo, I. Picomolar Inhibition of Plasmepepsin V, an Essential Malaria Protease, Achieved Exploiting the Prime Region. *PLoS One* **2015**, 10 (11), No. e0142509, DOI: 10.1371/journal.pone.0142509.

(37) Gazdik, M.; O'Neill, M. T.; Lopaticki, S.; Lowes, K. N.; Smith, B. J.; Cowman, A. F.; Boddey, J. A.; Sleebs, B. E. The Effect of N-Methylation on Transition State Mimetic Inhibitors of the Plasmodium Protease, Plasmepepsin V. *Med. Chem. Commun.* **2015**, 6 (3), 437–443.

(38) Bobrovs, R.; Jaudzems, K.; Jirgensons, A. Exploiting Structural Dynamics To Design Open-Flap Inhibitors of Malarial Aspartic Proteases. *J. Med. Chem.* **2019**, 62 (20), 8931–8950.

(39) Rasina, D.; Stakanovs, G.; Kanepe-Lapsa, I.; Bobrovs, R.; Jaudzems, K.; Jirgensons, A. Synthesis of 2-Aminopyridopyrimidiones and Their Plasmepepsin I, II, IV Inhibition Potency. *Chem. Heterocycl. Compd.* **2020**, 56 (6), 786–792.

(40) Zogota, R.; Kinena, L.; Withers-Martinez, C.; Blackman, M. J.; Bobrovs, R.; Pantelejevs, T.; Kanepe-Lapsa, I.; Ozola, V.; Jaudzems, K.; Suna, E.; Jirgensons, A. Peptidomimetic Plasmepepsin Inhibitors with Potent Anti-Malarial Activity and Selectivity against Cathepsin D. *Eur. J. Med. Chem.* **2019**, 163, 344–352.

(41) Kinena, L.; Leitis, G.; Kanepe-Lapsa, I.; Bobrovs, R.; Jaudzems, K.; Ozola, V.; Suna, E.; Jirgensons, A. Azole-Based Non-Peptidomimetic Plasmepepsin Inhibitors. *Arch. Pharm.* **2018**, 351, No. 1800151, DOI: 10.1002/ardp.201800151.

(42) Rasina, D.; Stakanovs, G.; Borysov, O. V.; Pantelejevs, T.; Bobrovs, R.; Kanepe-Lapsa, I.; Tars, K.; Jaudzems, K.; Jirgensons, A. 2-Aminoquinazolin-4(3H)-One Based Plasmepepsin Inhibitors with Improved Hydrophilicity and Selectivity. *Bioorg. Med. Chem.* **2018**, 26 (9), 2488–2500.

(43) Rasina, D.; Otkovs, M.; Leitans, J.; Recacha, R.; Borysov, O. V.; Kanepe-Lapsa, I.; Domraceva, I.; Pantelejevs, T.; Tars, K.; Blackman, M. J.; Jaudzems, K.; Jirgensons, A. Fragment-Based Discovery of 2-Aminoquinazolin-4(3H)-Ones As Novel Class Non-peptidomimetic Inhibitors of the Plasmepepsins I, II, and IV. *J. Med. Chem.* **2016**, 59 (1), 374–387.

(44) Friedman, R.; Cafisch, A. The Protonation State of the Catalytic Aspartates in Plasmepepsin II. *FEBS Lett.* **2007**, 581 (21), 4120–4124.

(45) Bobrovs, R.; Basens, E. E.; Drunka, L.; Kanepe, I.; Matisone, S.; Velins, K. K.; Andrianov, V.; Leitis, G.; Zelencova-Gopejenko, D.; Rasina, D.; Jirgensons, A.; Jaudzems, K. Exploring Aspartic Protease Inhibitor Binding to Design Selective Antimalarials. *J. Chem. Inf. Model.* **2022**, 62, 3263–3273, DOI: 10.1021/acs.jcim.2c00422.

(46) Geschwindner, S.; Olsson, L.-L.; Albert, J. S.; Deinum, J.; Edwards, P. D.; de Beer, T.; Folmer, R. H. A. Discovery of a Novel Warhead against  $\beta$ -Secretase through Fragment-Based Lead Generation. *J. Med. Chem.* **2007**, 50 (24), 5903–5911.

(47) Tribello, G. A.; Bonomi, M.; Branduardi, D.; Camilloni, C.; Bussi, G. PLUMED 2: New Feathers for an Old Bird. *Comput. Phys. Commun.* **2014**, 185 (2), 604–613.

(48) Tiwary, P.; Parrinello, M. A Time-Independent Free Energy Estimator for Metadynamics. *J. Phys. Chem. B* **2015**, 119 (3), 736–742.

(49) Gapsys, V.; Pérez-Benito, L.; Aldeghi, M.; Seeliger, D.; Van Vlijmen, H.; Tresadern, G.; De Groot, B. L. Large Scale Relative Protein Ligand Binding Affinities Using Non-Equilibrium Alchemy. *Chem. Sci.* **2020**, 11 (4), 1140–1152.

(50) Ceriotti, M.; Tribello, G. A.; Parrinello, M. Simplifying the Representation of Complex Free-Energy Landscapes Using Sketch-Map. *Proc. Natl. Acad. Sci. U.S.A.* **2011**, *108* (32), 13023–13028.

(51) Tribello, G. A.; Ceriotti, M.; Parrinello, M. Using Sketch-Map Coordinates to Analyze and Bias Molecular Dynamics Simulations. *Proc. Natl. Acad. Sci. U.S.A.* **2012**, *109* (14), 5196–5201.

(52) Bonomi, M.; Bussi, G.; Camilloni, C.; Tribello, G. A.; Banáš, P.; Barducci, A.; Bernetti, M.; Bolhuis, P. G.; Bottaro, S.; Branduardi, D.; Capelli, R.; Carloni, P.; Ceriotti, M.; Cesari, A.; Chen, H.; Chen, W.; Colizzi, F.; De, S.; De La Pierre, M.; Donadio, D.; Drobot, V.; Ensing, B.; Ferguson, A. L.; Filizola, M.; Fraser, J. S.; Fu, H.; Gasparotto, P.; Gervasio, F. L.; Giberti, F.; Gil-Ley, A.; Giorgino, T.; Heller, G. T.; Hocky, G. M.; Iannuzzi, M.; Invernizzi, M.; Jelfs, K. E.; Jussupow, A.; Kirilin, E.; Laio, A.; Limongelli, V.; Lindorff-Larsen, K.; Löhr, T.; Marinelli, F.; Martin-Samos, L.; Masetti, M.; Meyer, R.; Michaelides, A.; Molteni, C.; Morishita, T.; Nava, M.; Paissoni, C.; Papaleo, E.; Parrinello, M.; Pfaendtner, J.; Piaggi, P.; Piccini, G.; Pietropaolo, A.; Pietrucci, F.; Pipolo, S.; Provasi, D.; Quigley, D.; Raiteri, P.; Raniolo, S.; Rydzewski, J.; Salvalaglio, M.; Sosso, G. C.; Spiwok, V.; Sponer, J.; Swenson, D. W. H.; Tiwary, P.; Valsson, O.; Vendruscolo, M.; Voth, G. A.; White, A. Promoting Transparency and Reproducibility in Enhanced Molecular Simulations. *Nat. Methods* **2019**, *16* (8), 670–673.